Distinctive Occupancy of Brain Coupling Modes across Autism spectrum subtypes

Vânia Miguel[1], Miguel Farinha[2], Alvaro Deleglise[3], Jakub Vohryzek[4], Josephine Cruzat[5], Fran Hancock[6], Eloise Stark[7], Pedro Morgado[1,8,], Gustavo Deco[4,9], Morten Kringelbach[7,10], Joana Cabral[1,7,8,#]

[1] Life and Health Sciences Research Institute (ICVS), School of Medicine, University of Minho, Braga, Portugal

[2] Department of Computer Science, University of Oxford, United Kingdom

[3] Consejo Nacional de Investigaciones Científicas y Técnicas (CONICET), Buenos Aires, Argentina

[4] Computational Neuroscience Group, Center for Brain and Cognition, Universitat Pompeu Fabra, Spain.

[5] Latin American Brain Health Institute, Universidad Adolfo Ibañez, Santiago de Chile, Chile

[6] The Institute for Human and Synthetic Minds, King's College London, London, UK

[7] Centre for Eudaimonia and Human Flourishing, Linacre College, University of Oxford, United Kingdom

[8] ICVS-3Bs PT Government Associate Laboratory, Braga, Guimarães, Portugal

[9] Institució Catalana de la Recerca i Estudis Avançats (ICREA), Barcelona, Spain

[10] Center for Music in the Brain, Department of Clinical Medicine, Aarhus University, Aarhus, Denmark

[#] Correspondence: joanacabral@med.uminho.pt

Abstract

Spontaneous brain activity captured with functional magnetic resonance imaging (fMRI) at rest engages in distinct coupling modes over time, transiently forming functional networks. While these networks show promise as biomarkers for psychiatric conditions, our limited understanding of their fundamental organizing principles has constrained the development of network-targeted therapeutic interventions.

In this study, Leading Eigenvector Dynamics Analysis (LEiDA) is applied to fMRI scans from n=945 participants from the Autism Brain Imaging Data Exchange (ABIDE I), demonstrating sensitivity to discriminate Autism Spectrum Disorder (ASD) subtypes and neurotypical controls. Compared to neurotypical controls (n=508), participants with Autistic Disorder subtype (n=331) exhibited reduced occurrence of both the Default Mode Network, DMN, and the Frontoparietal Network. In contrast, participants with Pervasive Developmental Disorder subtype (n=31) show increased occurrence of a more diffuse DMN configuration involving temporal areas and a Salience-Somatomotor network, whereas participants with Asperger subtype (n=75) show a subtle reduction of Frontoparietal Network occupancy.

By detecting phase-alignment modes—a fundamental physical phenomenon characteristic of standing waves—LEiDA provides a novel perspective on how brain networks self-organize at rest. Building on this mechanistic foundation, LEiDA successfully identified reproducible differences in functional network occupancy among the distinct ASD subtype classifications. Beyond its demonstrated utility as a diagnostic tool, these findings reveal LEiDA's ability to characterize the principles through which brain networks achieve their complex spatiotemporal organization. Through its publicly available MATLAB and Python implementations, LEiDA offers researchers a powerful framework for investigating the physical mechanisms that shape functional brain dynamics in both health and disease.

1. Introduction

Brain activity captured with functional magnetic resonance imaging (fMRI) at rest exhibits spontaneous fluctuations that organize at the macroscale, during which the signals in distinct brain areas co-fluctuate together - coupling modes with functional relevance. Typically referred to as resting-state networks or intrinsic connectivity networks, these patterns are consistently and robustly detected in human resting-state fMRI, and appear altered in a wide range of psychiatric conditions, pointing to close relation with brain function (Biswal et al., 2010; Fornito et al., 2015; Fox & Raichle, 2007). Despite extensive research, the fundamental principles organizing these patterns of brain activity and driving their dynamics remain incompletely understood.

Among the diversity of analysis methods to quantify the expression of these patterns and evaluate differences between conditions, a particular algorithm, termed Leading Eigenvector Dynamics Analysis (LEiDA) is demonstrating growing potential given its remarkable sensitivity to capture alterations between psychiatric (Farinha et al., 2022; Figueroa et al., 2019; Hancock et al., 2023), pharmacological (Lord et al., 2019; Olsen et al., 2022), psychological (Alonso Martínez et al., 2020), and even task conditions (Alonso Martínez et al., 2020; Fasano et al., 2023; Stark et al., 2020), with demonstrated replicability across studies (Lord et al., 2019; Olsen et al., 2022). LEiDA offers a promising framework for uncovering brain dynamics in health and disease.

The distinctive capability of LEiDA lies in its ability to capture instantaneous coupling modes, defined in terms of the phase relationships between brain regions. These modes, conceptualized as vectors analogous to standing wave patterns, represent configurations where some brain regions co-vary in phase while others vary in anti-phase. By characterizing these modes in terms of their probabilities of occurrence during specific time intervals, LEiDA provides a statistically robust approach for comparing brain dynamics across conditions, groups, and individuals (Cabral et al., 2017). This sensitivity has positioned LEiDA as a valuable tool for identifying potential neuromarkers—measurable and unbiased characteristics of brain dynamics. Such biomarkers hold promise for improving diagnostics, monitoring therapeutic outcomes (theranostics), and predicting cognitive function.

In the literature, patterns of correlated brain activity have been referred to by various terms, including resting-state networks (RSNs) (Amemiya et al., 2023), intrinsic connectivity networks (ICNs) (Knyazev et al., 2020), co-activation patterns (CAPs) (Liu et al., 2018), and functional gradients (Katsumi et al., 2023). These terminologies reflect different analytical approaches and perspectives in studying brain connectivity. In this article, we adopt the term "coupling modes" to emphasize the dynamic and temporal aspects of brain region interactions, as captured by the LEiDA method. This terminology highlights temporarily stable phase relationships between brain regions (or phase-aligned coupling modes), providing a nuanced understanding of functional connectivity patterns.

Unlike other approaches, such as independent component analysis (ICA) (Lee, 1998), graph theory-based methods (Sporns, 2018), dynamic functional connectivity (dFC) (Xie et al., 2019), and hidden Markov models (HMM) (Vidaurre et al., 2018), which often focus on global network properties or sequential patterns, LEiDA explicitly identifies and quantifies the occurrence of discrete brain coupling modes. This specificity enables the detection of short-lived but critical changes in brain dynamics, directly linked to cognitive states, neurological disorders, or pharmacological effects. By providing a structured framework for distinguishing and quantifying recurrent coupling modeswith

distinct temporal profiles, LEiDA facilitates a deeper understanding of dynamic organization principles of brain networks and their roles in brain function and pathology.

Since its introduction in 2017 (Cabral et al., 2017), studies utilizing LEiDA have reported significant findings across various conditions. However, most previous investigations were limited by relatively small sample sizes. Validation across larger datasets and a wider spectrum of conditions is required to fully demonstrate the method's potential. To address this, the present study applied LEiDA to resting-state fMRI (rs-fMRI) data from the Autism Brain Imaging Data Exchange I (ABIDE I) repository. This dataset includes a large cohort of individuals, enabling the exploration of significant differences not only between neurotypical individuals and those with autism spectrum disorder (ASD) but also within ASD subtypes.

ASD is a complex neurodevelopmental condition encompassing a range of phenotypes characterized by varying degrees of social, communicative, and sensory impairments (Hodges et al., 2020; Oberman & Kaufmann, 2020). Current diagnostic tools for ASD rely predominantly on subjective evaluations of linguistic, social, and behavioral features, highlighting the need for more objective, data-driven approaches (Guthrie et al., 2013). Neuroscientific methods, including fMRI-based studies, offer the potential to map the intricate relationships between ASD-associated behavioral changes and underlying brain activity patterns, contributing to a more precise understanding of the disorder.

ASD encompasses multiple subtypes, including Autistic Disorder (AUT), Asperger syndrome (ASP), and pervasive developmental disorder-not otherwise specified (PDD-NOS), according to the classification used in the ABIDE I database (Di Martino et al., 2014). Although Asperger syndrome and PDD-NOS were previously classified separately, they are now grouped under the umbrella of ASD. These subtypes exhibit distinct phenotypic and functional profiles, with varying degrees of severity and unique associations with specific resting-state networks. For instance, Asperger syndrome is often characterized by milder symptoms, while PDD-NOS includes a broad range of atypical features (Oberman & Kaufmann, 2020). Investigating these subtypes through large-scale fMRI datasets offers an opportunity to verify if these behavioral phenotypes are related with distinctive modes of brain activity patterns. Such insights may provide mechanistic insight into the physiology of these syndromes and inform targeted interventions to improve well being for individuals across the autism spectrum.

This study aims to leverage LEiDA's sensitivity to detect and characterize differences in brain coupling modes across ASD subtypes. By analyzing data from ABIDE I, we seek to identify distinctive brain dynamics that reflect the diversity of ASD phenotypes, thereby advancing our understanding of the neural underpinnings of autism and its subtypes.

2. Results

2.1. Detection of Functionally-Relevant Coupling Modes

Applying the LEiDA method to resting-state fMRI data from 945 participants reveals a set of recurrent modes of coupling, most of which closely resemble canonical resting state networks described in previous literature. The recurrent modes detected with LEiDA are represented in Figure 1a, where each row represents the partition into a different number of states k and sorted from left to right according to their probability of occurrence across all participants. Each coupling mode is represented by the corresponding cluster centroid c, coloring only the subset of brain areas synchronizing together in phase, while shifted in phase from the rest of the brain.

Consistently, irrespective of the number of clusters considered, the mode with the highest probability of occurrence across scans is a global mode, in which the fMRI signals of all brain areas are aligned in phase, not revealing the segregation of any particular subsystem (hence represented as a transparent brain), occupying the first column of **Figure 1a**. The remaining modes exhibit the segregation of a subset of brain areas, within which the fMRI signals are synchronized together forming a functional network, while shifted out of phase from the rest of the brain. To relate the coupling modes detected with LEiDA with canonical functional networks, each coupling mode was compared with the seven ICNs defined in (Yeo et al., 2011) (**Figure 1b**), and colored according to the ICN with which they correlate the most. Despite the distinct methodologies, we observe strong similarity between the cluster centroids detected with LEiDA and the reference ICNs. However, this overlap is merely indicative, because contrary to ICNs, the same voxel can belong to more than one mode.

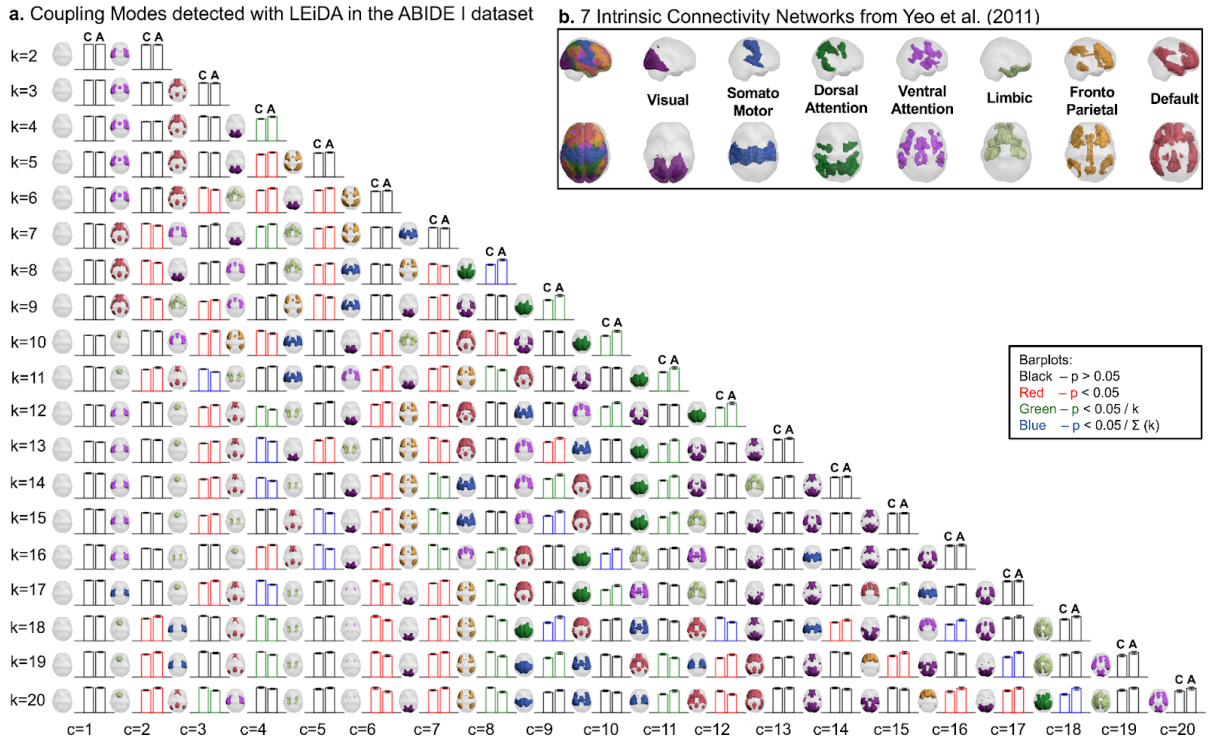

Figure 1. Coupling modes detected with LEiDA across all 945 participants, comparing their occurrence between participants from the Autistic Disorder subtype and neurotypical controls. a. *Pyramid showing all the phase coupling modes detected when applying k-means clustering to the entire sample of 180954 leading eigenvectors (from 945 fMRI scans, each with 75 to 313 time points), with the number of clusters K increasing from k = 2 (top) to k = 20 (bottom) clusters. The coupling modes are sorted from left to right according to their average occupancy across all scans. Each mode is represented by the corresponding cluster centroid (c) shown in a transparent brain viewed from the top, rendering the brain areas whose fMRI signals are shifted out of phase from the rest of the brain. Modes are colored according to the ICN defined by Yeo et al. (2011) (shown in b.) with which they correlate most significantly ($p < 0.05/K$).Modes not overlapping with any of the reference ICNs are colored in black. For each mode, bar plots indicate the mean fractional occupancy in the Control (C) group and the Autistic Disorder (A) group. Red, green and blue bar plots indicate the degree of statistical significance, ranging from $p < 0.05$ (higher chance of false positives), $p < 0.05 / k$ and $p < 0.05 / \Sigma(k)$ (surviving the most conservative Bonferroni correction), respectively. Black barplots indicate no difference detected between groups ($p > 0.05$).* ***b.*** *Seven intrinsic Connectivity Networks defined in Yeo et al., (2011).*

All seven ICNs defined in (Yeo et al., 2011) are detected for partitions into k=8 and above (**Figure 2**). This finding emphasizes LEiDA's capability in differentiating and mapping out the brain modes of coupling aligning with canonical functional network architectures. As the number of clusters k is increased, finer grained subdivisions give the possibility of more subtle distinctions between coupling

modes. From k=9, more than one mode may overlap with the same ICN. For example, the two coupling modes detected with k=11 overlapping with the DMN (c=3 and c=9) are distinguished by the synchrony (or not) with areas in the frontal and temporal lobes.

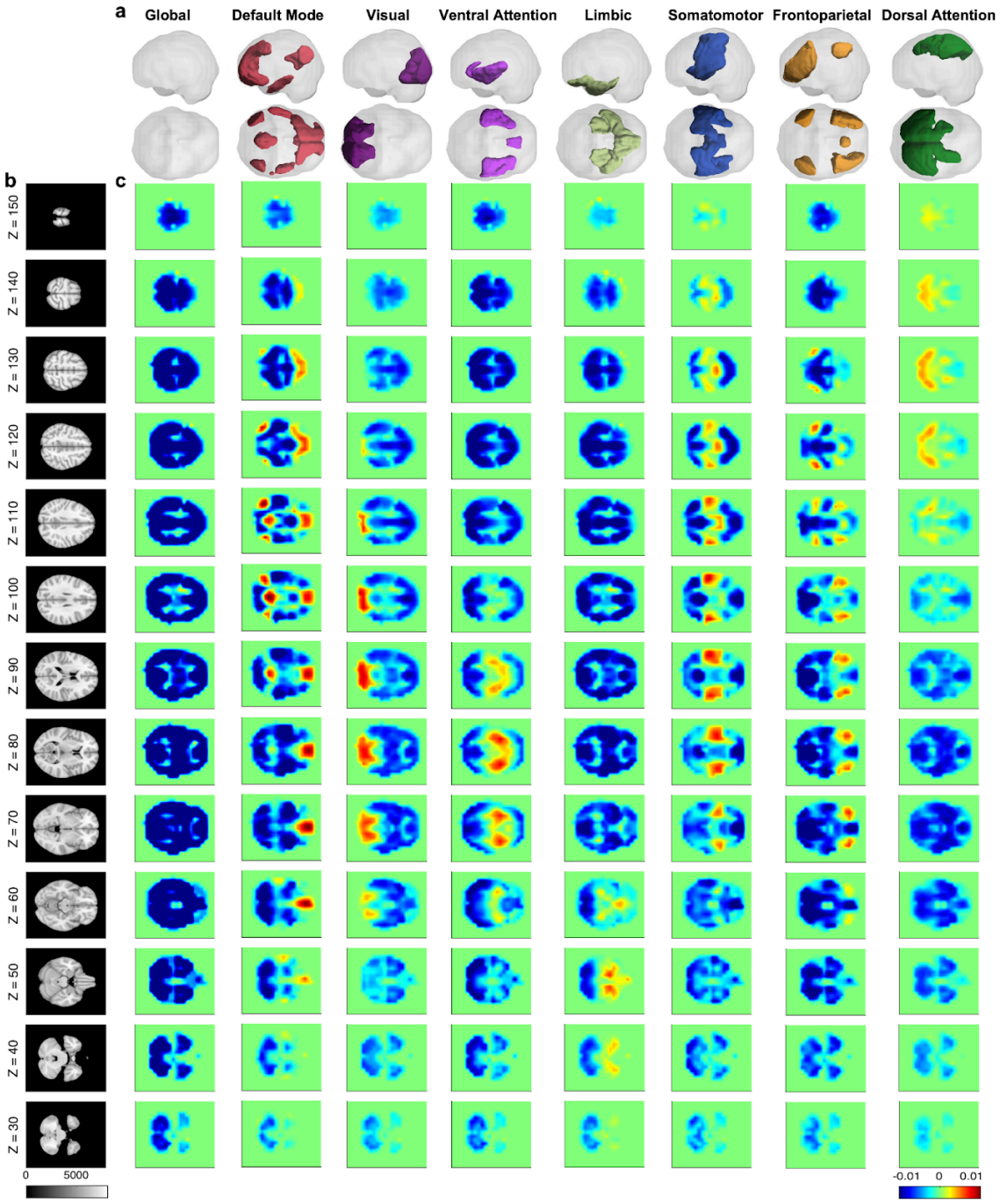

Figure 2. Coupling modes obtained for k=8 visualized in MNI space. *(**a**) Coupling modes shown in transparent brains (top and side views) coloring the voxels whose signals shift out of phase from the rest of the brain (same color code from Fig1b). (**b**) 13 axial slices of a T1-weighted MNI brain scan. (**c**) Each coupling mode is obtained in MNI space (see Methods for details) and shown for the same 13 axial slices from (**b**) (areas forming a segregated functional network are highlighted in warmer colours, cool coloured bars represent brain areas in anti-phase to the ones highlighted).*

2.2. Distinctive occupancy of Coupling Modes across ASD subtypes

For each fMRI scan, we quantify the temporal prevalence of coupling modes by counting the number of timepoints when each mode is dominant. This allows comparing mode occupancy between groups, which reveals significant differences in several modes between neurotypical participants and individuals with distinct ASD subtypes (complete between-group statistical analysis, including p-values and effect sizes, are reported in **Supplementary Material Figures S1-S9**).

The most significant differences in mode occupancy are detected between neurotypical controls and participants with Autistic Disorder (bar plots shown next to each cluster centroid in **Figure 1**, where the blue color indicates significant differences surviving Bonferroni correction for all the 209 comparisons performed, i.e. $p < 0.05/209=0.00024$). For a range of k, the default mode network (DMN) emerged as the most distinctive network between groups, consistently occurring less often in participants with Autism when compared to neurotypical participants (blue bar plots for k=11, 13, 14, 15, 16 and 17 in **Figure 1**). Conversely, two other modes were found to occur more often in participants with Autistic disorder than in neurotypical controls, one revealing the Dorsal Attention Network (DAN, blue bar plots for k=8, 16, 18 and 20 in **Figure 1**) and another revealing the Ventral Attention Network (VAN, k=15 and 18). These coupling modes will be described in detail in section 2.2.1.

Differences in mode occupancy were less significant when comparing all the other group pairs (**Supplementary Material Figures S1-S9**). Still, participants in the PDD-NOS group exhibited differences from neurotypical controls and participants with Asperger's syndrome with moderate effect sizes (Hedge's $g > 0.5$) and survived the adjusted threshold of $p < 0.05/k$, which corrects for the number of independent comparisons performed in each partition. These coupling modes distinguishing between ASD subtypes will be described in section 2.2.2.

2.2.1. Distinctive Coupling Modes in Autistic Disorder subtype

The most significant difference between all conditions compared was observed between CONT and AUT in the occurrence of a coupling mode involving key regions of the Default Mode Network (DMN), namely the posterior cingulate cortex, bilateral angular gyrus, medial orbitofrontal cortex and and medial frontal gyrus (listed in **Figure 3d**, sorted based on the phase projection into V1). This mode (detected with the highest precision with k=16), occurred on average 7.45%$\pm$0.18% (Mean $\pm$ Standard Error of the Mean (SEM)) in neurotypical controls and 6.2%$\pm$0.20% of the time in participants in the Austism subtype group (p_{perm}=0.00000026, p_{corr}=0.000054, effect size (g=0.314). Participants in the PDD-NOS group also exhibit a lower occupancy of this coupling mode, i.e., 5.7%$\pm$ 0.68%, although with higher variability and differing only weakly from controls (p_{perm}=0.027, Effect size g=0.404 although not surviving Bonferroni correction). This indicates an altered or disrupted performance of this network in individuals from the autism subtype, showing a similar trend in individuals in the PDD-NOS group.

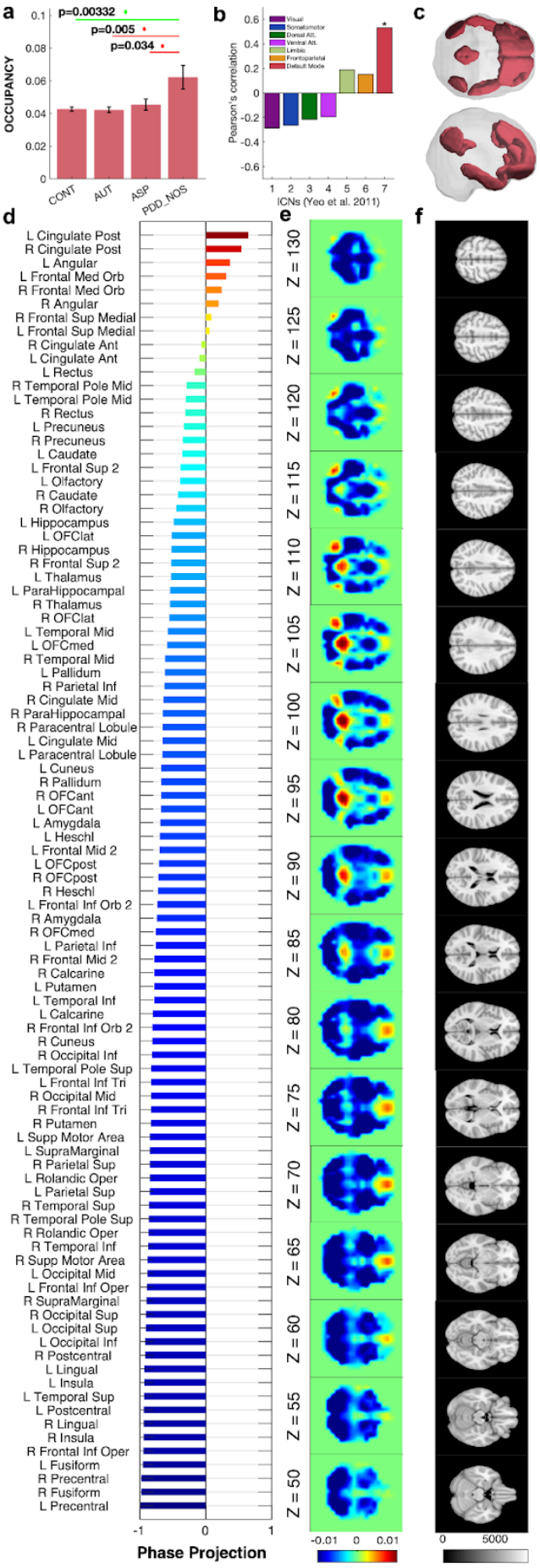

Figure 3. Coupling Mode found to most significantly distinguish participants from the Autistic Disorder subtype and Neurotypical Controls. ***(a)*** *Mean fractional occupancy of mode k=16 c=5 in each condition (CONT, neurotypical controls, AUT, autistic disorder, ASP, Asperger syndrome and PDD_NOS, pervasive development disorder not otherwise specified). Error bars represent the standard error of the mean (SEM). Differences between conditions are reported when p<0.05.* ***(b)*** *Correlations with 7 reference ICNs defined in Yeo et al., (2011).* ***(c)*** *Coupling mode represented in a transparent brain, rendering the smallest subset of voxels synchronizing together, coloured according to the ICN to which they overlap the most.* ***(d)*** *List of 94 brain areas of the AAL2 atlas and the corresponding projection into the leading eigenvector (areas forming a segregated functional network are highlighted in warmer colours).* ***(e)*** *17 axial slices of the coupling mode obtained in MNI space (see Methods for details). Colors represent the phase projection.* ***(f)*** *T1-weighted MNI brain template shown for the same 17 axial slices from* ***(e)****.*

The reduction in DMN occupancy observed in participants with Autistic Disorder is accompanied by an increased occupancy of coupling modes overlapping slightly (Pearson's correlation coefficient < 0.4) with the DAN, the VAN and the Visual Network (**Figure 4**). Irrespective of the ICNs to which they correlate, visualizing these modes in axial slices reveals that these modes are characterized by correlated fMRI signals in widely distributed areas covering either, dorsal (**Figure 4d**), ventral (**Figure 4h**) or posterior (**Figure 4l**) parts of the brain, evolving out of phase from the rest of the brain.

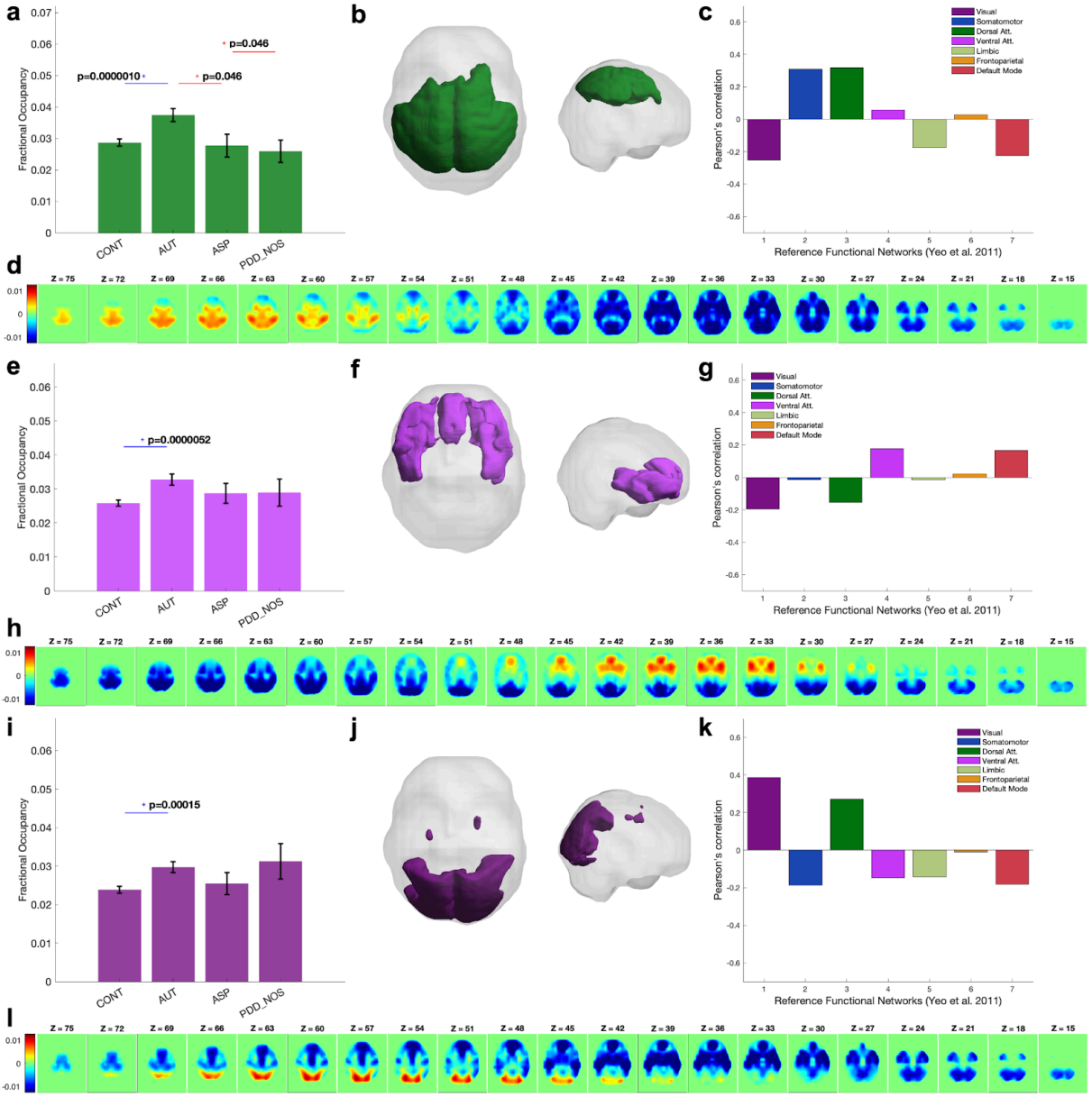

Figure 4 - Coupling Modes occurring differently in the Autistic subtype (a, e, i) *Mean fractional occupancy in each condition (CONT, neurotypical controls; AUT, autistic disorder; ASP, Asperger syndrome; and PDD-NOS, pervasive developmental disorder not otherwise specified), reporting significant p-values (red p<0.05, blue p<0.00024). Bars represent the standard error of the mean (SEM).* ***(b, f, j)*** *Representation of the coupling modes inside a transparent brain in top and side views, rendering the voxels whose signals shift out of phase form the rest of the brain, coloured according to the ICN to which they correlate the most.* ***(c, g, k)*** *Correlation between the cluster centroids and ICNs. (2011).* ***(d, h, l)*** *Cluster centroids obtained in MNI space and represented in equidistant axial slices, with red to blue colors representing positive to negative elements in the vector representing each mode.*

2.2.2. Distinctive Coupling Modes in PDD-NOS

Participants diagnosed with PDD-NOS differentiated mostly from all other conditions in a coupling mode overlapping with the DMN (k=14, c=10) (**Figure 5b**). This DMN configuration not only includes the same key areas presented in **Figure 3**, but also couples with a more extensive network of brain regions including the entire orbitofrontal cortex (extending to lateral, intermediate, posterior and inferior parts), as well as the olfactory cortex, the anterior cingulate cortex, the mid and superior frontal cortex, the gyrus rectus, and the caudate, all bilaterally involved. This pattern occurred around

6.2%±0.72% of the time in participants with PDD-NOS, compared to 4.3%±0.13% in neurotypical controls (p=0.0033, Hedge's g=0.62), 4.2%±0.17% in the Autism group (p=0.0048 , g=0.62), and 4.5%±0.33% in the Asperger group (p=0.034, g=0.51).

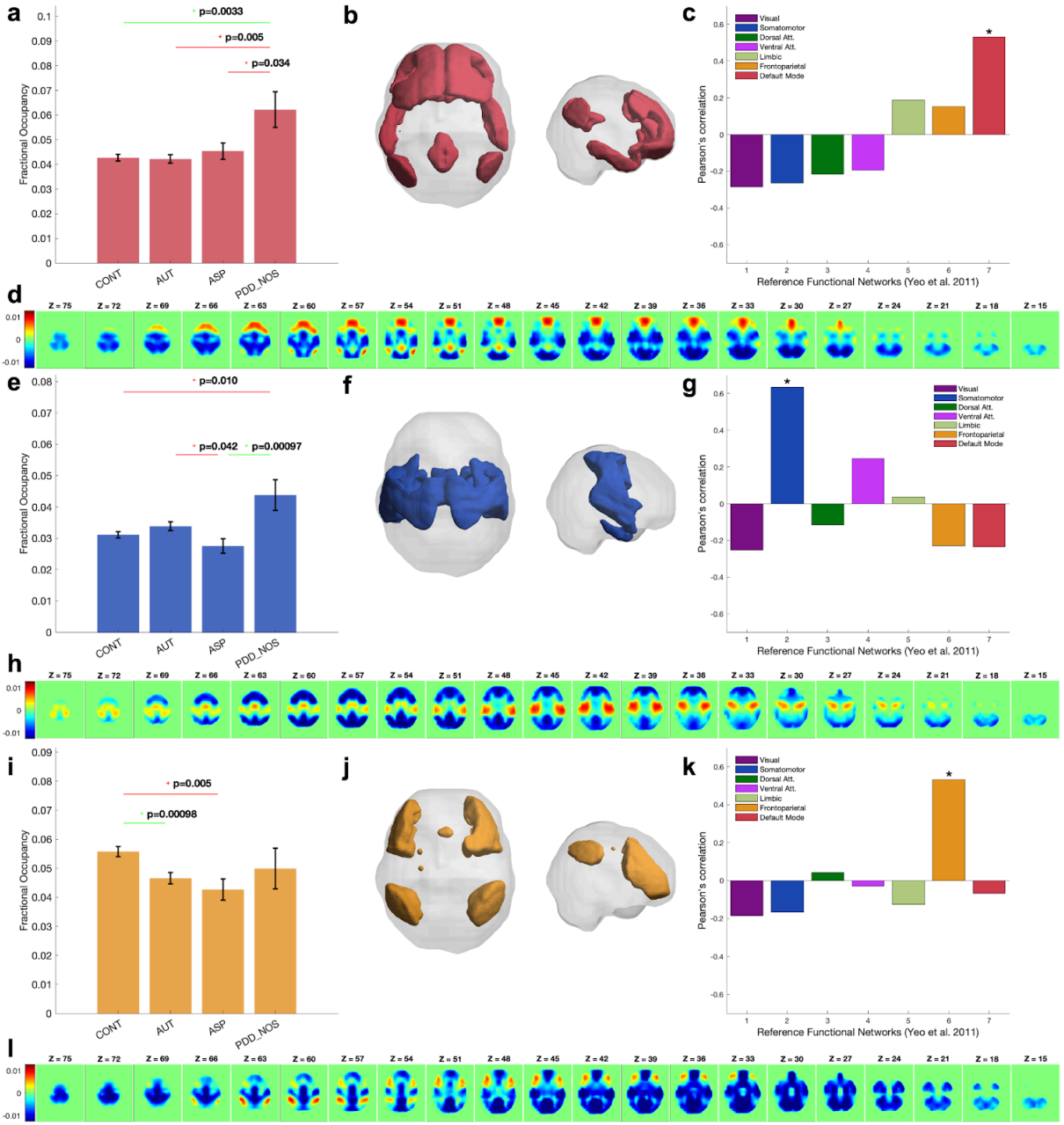

Figure 5. Coupling Modes occurring differently across ASD subtypes. (a; e; i) *Mean fractional occupancy in each condition (CONT, neurotypical controls; AUT, autistic disorder; ASP, Asperger syndrome; and PDD-NOS, pervasive developmental disorder not otherwise specified), reporting only significant p-values for statistical comparisons between conditions. Bars represent the standard error of the mean (SEM).* ***(b; f; j)*** *Coupling mode represented in a transparent brain, rendering the smallest subset of voxels synchronizing together, coloured according to the ICN to which they overlap the most.* ***(c; g; k)*** *Bar plots identifying and quantifying significant correlations between the modes detected and reference functional networks, as defined by Yeo et al. (2011).* ***(d; h; l)*** *Segregated functional networks displayed on axial brain slices in MNI space, with warm to cool colors representing synchrony in-phase or anti-phase, respectively.*

2.2.3. Distinctive Coupling Modes in Asperger's syndrome

When comparing the brain scans from participants with Asperger's syndrome subtype with the other groups, the strongest difference consists in reduced detection of a network overlapping with the Somatomotor network (k=16 and c=14, **Figure 5**, middle panel). This difference was stronger when comparing with individuals with PDD-NOS (p=0.00097, g=0.72), where this network was detected around 4.4% ± 0.49% of the time compared to 2.8% ± 0.23% in participants with Asperger's syndrome. Participants from the Autistic subtype group also tend to exhibit this mode often (3.4% ± 0.14%) compared to participants in the Asperger's syndrome group (p=0.042, g=0.26).

Finally, a mode overlapping with the frontoparietal network (**Figure 5** bottom panel, mode obtained with k=18, c=8), occurred more often in neurotypical controls (5.6% ± 0.18%) when compared to participants from the Autistic Disorder subtype (4.7% ± 0.20%, p=0.0098, g=0.33). Although the mean occupancy of this mode is even lower across individuals with Asperger's syndrome (4.3% ± 0.36%), this reduction was less significant (p=0.0046, g=0.24), not surviving correction for the number of independent modes (k=18) compared.

3. Discussion

The relationship between the brain's activity and the emergence of cognition and behavior remains one of neuroscience's most complex questions. While we know the mind arises from the brain, the exact mechanisms linking functional connectivity patterns to behavioral and cognitive outcomes are far from understood. Resting-state fMRI provides a window into this activity, capturing spontaneous fluctuations in brain regions that may offer insights into the organization of brain networks. However, the complexity and dynamism of these signals make them difficult to interpret, particularly when trying to link them to cognitive and behavioral outcomes.

Large-scale datasets like ABIDE I, paired with innovative methods like Leading Eigenvector Dynamics Analysis (LEiDA), allow us to navigate these complexities. By separating individuals into groups defined by cognitive and behavioral traits, we gain a unique opportunity to identify patterns of brain activity that correlate with these differences. Our investigation leverages this framework to explore how brain coupling modes vary within ASD subtypes and neurotypical controls, offering a fresh perspective on the dynamic organization of brain networks.

The observed differences in coupling mode occupancy across groups highlight LEiDA's sensitivity in capturing short-lived but critical changes in brain dynamics. By identifying distinct coupling modes with strong statistical power, this study supports LEiDA's potential as a tool for discovering biomarkers. These biomarkers could provide objective measures to aid in ASD diagnosis, complementing subjective behavioral assessments, and offer new metrics for evaluating therapeutic interventions for the most debilitating subtypes.

Psychiatric conditions like ASD vary widely in their phenotype, with individuals presenting unique cognitive and behavioral characteristics. While some individuals with ASD function highly, others face severe challenges that profoundly impact their quality of life. Understanding the causes and processes behind these differences is crucial, especially given the limited availability of effective solutions for the most debilitating subtypes. Advances in mapping brain dynamics may provide critical insights into the mechanisms underlying these subtypes, informing more tailored interventions and improving outcomes for individuals across the spectrum.

3.1. Distinct Brain Coupling Modes in ASD Subtypes

Our results identified several recurrent coupling modes across neurotypical and ASD groups, with notable differences in their temporal prevalence. Consistently with previous research, the Default Mode Network (DMN) emerged as the most affected network in individuals with Autistic Disorder (AUT), showing reduced occupancy compared to neurotypical controls(Washington et al., 2014). This aligns with the well-documented role of DMN in social cognition and introspection(Li et al., 2014), functions that are often impaired in autism(Li et al., 2014; Ronde et al., 2024). Interestingly, other coupling modes, subtly linked to the Dorsal Attention Network (DAN), the Ventral Attention Network (VAN) and the visual network, occurred more frequently in the AUT group, suggesting a potential compensatory mechanism or an over-reliance on externally oriented attention.

While the DMN has been a focal point in ASD research ("The Default Mode Network in Autism," 2017), our analysis extends its scope by characterizing coupling modes specific to ASD subtypes. For instance, individuals with PDD-NOS exhibited distinctive DMN configurations, with additional engagement of orbitofrontal and cingulate regions. These findings suggest that the heterogeneity in PDD-NOS phenotypes is reflected in unique brain dynamics, emphasizing the need for further studies to decode these patterns.

Asperger syndrome (ASP), on the other hand, was weakly associated with coupling modes involving the Somatomotor and the Frontoparietal network. These modes showed differences when compared to both PDD-NOS and AUT subgroups, highlighting the variability in sensory and cognitive processing within the autism spectrum. Such findings underscore the importance of moving beyond a single-diagnosis framework to better understand ASD's diverse neural underpinnings.

While insights derived from resting-state fMRI data on Autism Spectrum Disorder (ASD) are compelling, it is important to note that causal relationships cannot yet be firmly established. The observed patterns may not necessarily indicate direct causality between neuronal processes and behavior, but they might also be secondary effects of other physiological phenomena (e.g., autonomic regulation, neurovascular coupling).

3.2. Challenges and Limitations

A significant limitation of this study arises from the temporal resolution of the fMRI data used. The repetition time (TR) of the scans varied across sites, ranging from 1500 ms to 3000 ms, with an average of 2 seconds. While this variability allows for broader inclusion of data, it poses challenges in achieving consistent temporal sampling across participants. With a TR averaging around 2 seconds, the study only captures a "snapshot" of brain activity at intervals that may fail to reflect more rapid changes in brain function. Emerging evidence suggests that finer temporal resolutions are necessary to fully characterize fast transitions between brain states and fluctuations within RSNs. Future studies should consider acquiring data with higher temporal resolution, such as via multiband echo-planar imaging (Cahart et al., 2022) or by reducing the number of slices (Cabral et al., 2023), to capture these subtler temporal changes more accurately and to resolve debates about their physiological significance.

Another challenge stems from the multisite nature of the ABIDE I dataset. Although pooling data from 16 international imaging sites increases sample size and generalizability, it also introduces

variability in scanner types, acquisition parameters, and preprocessing strategies. This variability can confound comparisons between individuals and groups, despite standardized preprocessing pipelines. While efforts were made to mitigate such inconsistencies (e.g., spatial normalization to MNI space and motion correction), residual site-specific biases may still influence the observed differences. Future work may benefit from advanced harmonization techniques, such as ComBat or domain adaptation models, to reduce site-related variability and enhance the robustness of cross-site analyses.

The absence of global signal regression (GSR) in our preprocessing approach also presents a potential limitation. Although GSR is a widely debated preprocessing step, it has been shown to reduce global noise, such as physiological artifacts from heart rate and respiration. By omitting GSR, we aimed to preserve the full spectrum of coupling modes. However, this choice leaves open the possibility that some of the variance attributed to coupling modes or behavioral correlations might be influenced by residual global noise. Future studies could investigate the impact of GSR more systematically to balance noise reduction with signal preservation.

The choice of spatial parcellation also warrants discussion. Averaging voxel signals within predefined brain regions reduces computational complexity but inherently assumes that each region is functionally homogeneous. This assumption may oversimplify complex dynamics, particularly in regions known for heterogeneous functional organization, such as the prefrontal cortex. Additionally, the resolution of the parcellation template used in this study may limit the ability to detect finer-grained spatial patterns of functional connectivity. Higher-resolution parcellation or voxel-wise approaches could provide more detailed insights into localized brain dynamics.

Lastly, our reliance on resting-state data constrains our ability to infer causal relationships. The study identified significant associations between coupling mode occupancy and phenotypic classification, yet the underlying causal mechanisms remain unclear. Without additional task-based fMRI or longitudinal data, it is impossible to determine whether the observed network dynamics directly drive behavioral differences or are merely epiphenomenal. This limitation underscores the need for multimodal approaches that combine resting-state fMRI with other modalities, such as EEG or MEG, to triangulate the physiological origins of these coupling modes.

3.3. Conclusions and Future Directions

This study demonstrates the power of LEiDA in identifying distinct patterns of brain activity across ASD subtypes and neurotypical controls, offering a new perspective on the dynamic organization of brain networks. The observed differences in coupling mode occupancy have important implications for our understanding of ASD, as well as for the development of new diagnostic tools and therapeutic strategies in phenotypes that compromise well-being. While the study provides valuable insights, further research is needed to address its limitations and to deepen our understanding of how these coupling modes relate to behavioral and cognitive outcomes. The identification of dynamic biomarkers for ASD holds significant promise for improving both diagnosis and treatment, paving the way for more personalized care for individuals across the autism spectrum.

4. Methods

4.1. Neuroimaging data, preprocessing and LEiDA configuration

In the current work we used data from the Autism Brain Imaging Data Exchange (ABIDE) (Craddock et al., 2013) released under the Preprocessed Connectomes Project (PCP) (http://preprocessed-connectomes-project.org/abide/index.html). The ABIDE I Preprocessed repository is a collaboration of 16 international imaging sites that have openly shared neuroimaging data which was subsequently preprocessed using four different preprocessing pipelines, each of which was implemented using the chosen parameters and settings of the pipeline developers.

We analyzed the resting-state fMRI data preprocessed using the Data Processing Assistant for Resting-State fMRI (DPARSF) containing a total of 945 participants, of which 508 neurotypical controls (C), 331 autism (AUT) patients, 75 participants with Asperger's syndrome (ASP) and 31 participants with pervasive developmental disorder - not otherwise specified (PDD-NOS)(Craddock et al., 2013). Basic preprocessing of the fMRI data included dropping the first 4 volumes of each scan, slice-timing correction and motion realignment. Regarding nuisance variable regression: (1) head motion effects were regressed from the realigned data using the Friston 24-parameter model(Friston et al., 1996) (i.e., 6 head motion parameters, 6 head motion parameters one time point before, and the 12 corresponding squared items), (2) confounding variation due to heartbeat and respiration was cleaned by regressing out the signals from white matter and cerebrospinal fluid, and (3) linear and quadratic trends were also included as regressors to account for low-frequency scanner drifts.

We selected the preprocessing strategy which did not include global signal regression (GSR) and temporal filtering because these procedures would extract further fMRI signal variance whose contribution to functional networks remains under debate (Chen, J. E., Lewis, L. D., Chang, C., Tian, Q., Fultz, N. E., Ohringer, N. A., Rosen, B. R., & Polimeni, J. R., 2020) and because previous studies using LEiDA revealed that considering the whole-frequency spectrum improves within-subject reliability regarding the temporal expression of coupling modes (Vohryzek et al., 2020). Finally, the functional volumes were registered to the MNI space at a 3 mm isotropic resolution and spatially smoothed with a 6-mm full-width at half-maximum (FWHM) Gaussian kernel.

Although LEiDA can be applied directly to the brain voxel time series, previously parcellating the data allows reducing computational cost. To reduce computational complexity, the rs-fMRI data were parcellated into 94 cortical and subcortical non-cerebellar regions using the Automated Anatomical Labeling Atlas 2 (AAL2). For each region, the fMRI signals were averaged over all voxels belonging to that area, resulting in an N×T dataset for each subject, where N is the number of brain areas and T is the number of time points in the scan.

4.2. Capturing fMRI Phase Dynamics

The instantaneous phase $\Theta(n.t)$ of the fMRI signal in each brain region $n \in \{1,\ldots,N\}$ and for each time $t \in \{2,\ldots,T-1\}$, is estimated using the Hilbert transform (Glerean et al., 2012), excluding the first and last time points to exclude the boundary artifacts induced by the Hilbert transform (Lord et al., 2019; Vohryzek et al., 2020). The Hilbert transform captures the time-varying phase of a fMRI signal at each time, t, by converting it into its analytical representation in the complex domain (**Figure 6a**). For some signal processing applications, such as the quantification of amplitude/power fluctuations in a given carrier frequency, it is necessary to filter the signals in a narrow frequency band before applying the Hilbert transform, according to the Bedrosian theorem. However, previous studies

using LEiDA have shown that performing the Hilbert transform to the unfiltered fMRI time series captures reliable phase coupling modes, without requiring to define a narrow frequency range, which could otherwise discard meaningful signals given the natural variability of frequencies between individuals.

4.3. System-Level Phase Dynamics captured by the Leading Eigenvector

The evolution of phases over space and time can be described with reduced dimensionality by considering only the leading eigenvector, $V_1(t)$, of the phase coherence matrix calculated at every time point t (Cabral et al., 2017). Specifically, for each pair of brain areas n and p, we compute the cosine of the phase difference between them, resulting in a symmetric NxN matrix, such that values close to 1 indicate the two areas n and p are in phase, -1 indicate they are in anti-phase, and 0 indicate they are shifted by 90º. By definition, this is a rank 2 matrix, with two eigenvectors, each with an associated real eigenvalue, and therefore all the phases can be described by their projection into these 2 eigenvectors without losing information (de Alteriis et al., 2024).

LEiDA considers only the eigenvector with largest eigenvalue, referred to as *leading* eigenvector, $V_1(t)$, which is a $N \times 1$ vector that captures the main orientation of phases across the entire brain at time t (Cabral et al., 2017). This approach has revealed high sensitivity to capture meaningful functional networks in previous studies (Stark et al., 2020). When all elements of $V_1(t)$ have the same sign, the phases between brain regions are coherent, which indicates a globally coherent mode governing all fMRI signals. Contrarily, if the elements of $V_1(t)$ have different signs (i.e., positive and negative), the signals recorded from the brain can be separated into two groups, evolving out of phase from each other. Additionally, the absolute value of each element in the leading eigenvector weighs the contribution of each brain area to the assigned group (Cabral et al., 2017; Newman, 2006). Based on previous LEiDA studies, we consider the smallest subset of brain areas shifting out of phase from the rest of the brain to form a functional network.

In total, 180954 'instantaneous' leading eigenvectors were obtained from all the 945 scans, each representing how the fMRI signals in all the N=94 brain areas are organized in terms of phase alignment at a given instant of time (**Figure 6**).

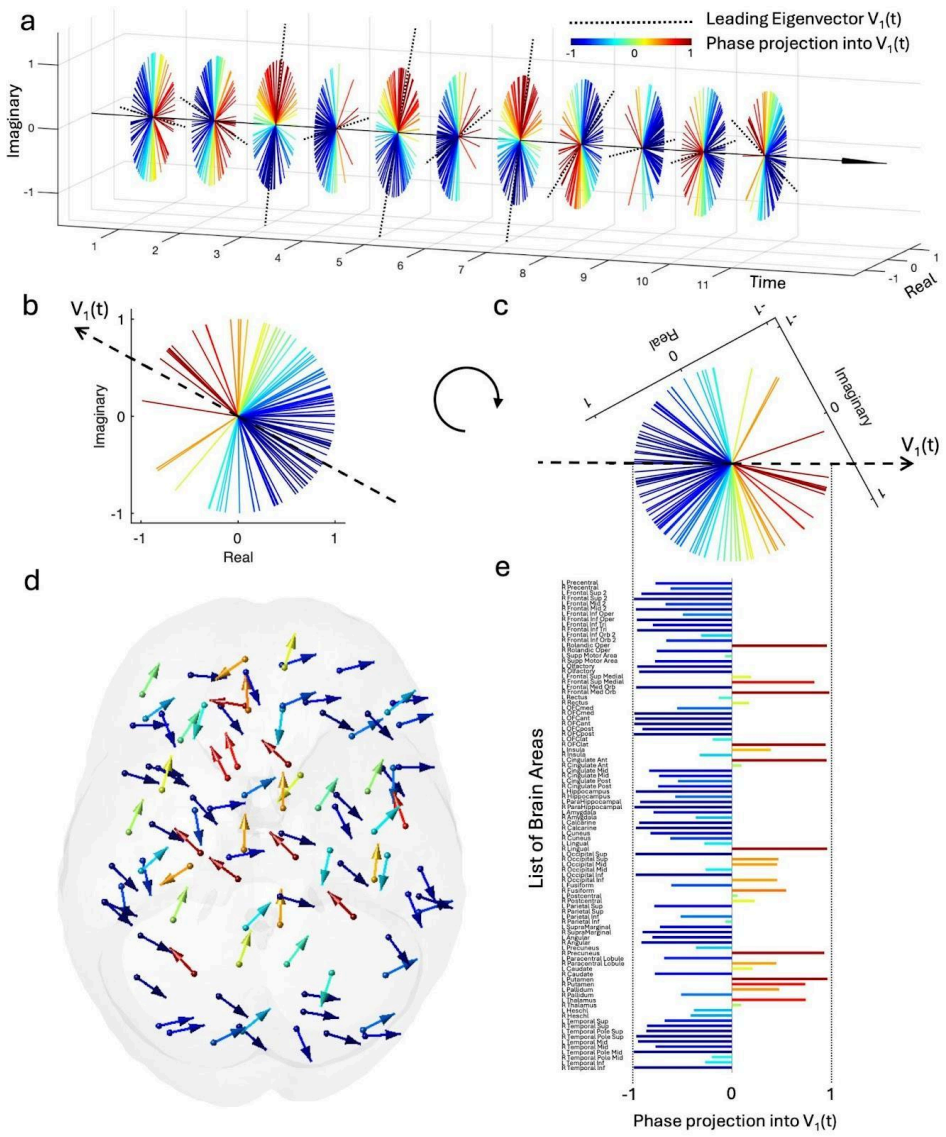

Figure 6 - System-Level Phase Dynamics captured by the Leading Eigenvector over time. a. *The fMRI signal phases in all N=94 brain areas are plotted over 11 consecutive time points, and colored according to the projection into the leading eigenvector, $V_1(t)$, represented as a black dashed line, whose orientation changes at each time point.* ***b.*** *Each of the 94 fMRI signal phases in the 11th time point are plotted in the complex plane, where the real axis corresponds to the cosine of the phase, and the imaginary axis corresponds to its sine. The largest magnitude eigenvector of the phase coherence matrix consists in an undirected vector that maximizes the sum of the projection of all phases. We define a direction by considering that the largest portion of phases project on the negative side (blue), and the smallest group of phases project on the positive direction (red).* ***c.*** *Change of axis by rotating the phase plane using the largest magnitude eigenvector as a reference axis.* ***d.*** *Each of the 94 fMRI signal phases in the 11th time point (same as* ***b****) are represented as arrows on a transparent brain placed at the center of gravity of each brain area, and colored according to their projection into $V_1(t)$.* ***e.*** *The eigenvector $V_1(t)$ is a 1xN vector, where the value in each element corresponds to the projection of the signal phase in each brain area into the leading eigenvector (as illustrated by panel* ***c*** *above).*

4.4. Clustering of Leading Eigenvectors

We identify recurrent coupling modes from the sample of 180954 leading eigenvectors by partitioning the sample into a set of k discrete clusters using a clustering algorithm (Cabral et al., 2017).

Here, we use the K-means algorithm to obtain the repertoire of coupling modes, although it has been shown that other clustering algorithms produce similar findings (Cabral et al., 2017; Farinha et al., 2022; Olsen et al., 2022). The K-means algorithm is run varying the number of clusters k from 2 to 20, i.e., dividing the set of leading eigenvectors into $k = 2, 3, ..., 2$ clusters, and using the cosine distance as the distance metric for minimization (Cabral et al., 2017). We selected the optimal solution from 1000 replicates to ensure stability of the results. Each cluster obtained using the K-means algorithm is represented by its centroid, which corresponds to the mean of all the leading eigenvectors belonging to that cluster (Aggarwal & Reddy, 2018).

For each value of k, the clustering procedure assigns each of the 180954 leading eigenvectors to one of k clusters, without distinguishing between participant groups or conditions. Each of the k clusters has a centroid, obtained as the mean of all the leading eigenvectors assigned to that cluster. This centroid, with size 1xN, represents a recurrent Coupling Mode.

4.5. Fractional Occupancy

The fractional occupancy (probability of occurrence) of a coupling mode α represents the proportion of time t that $V_1(t)$ is assigned to cluster C_α throughout a scan. The fractional occupancy of coupling mode α for the fMRI scan of subject s, $P^{(s)}_\alpha$, is estimated as follows:

$$P^{(s)}_{\alpha} = \frac{1}{T-2}\sum_{t=2}^{T-1} \mathbb{1}_{\{V_t^{(s)} \in C_\alpha\}}, \ \alpha \in \{1, ..., K\} \qquad (2)$$

where T is the number of time points (first and last volume of each scan are excluded), $\mathbb{1}$ is the indicator function and V_t is the coupling mode to which $V_1(t)$ is assigned at time t. For each clustering solution, this measure is estimated for each of the K PL states separately for each fMRI scan.

4.6. Intergroup comparisons

Hypothesis tests were performed to compare the group mean using Monte Carlo permutation tests (Aggarwal & Reddy, 2018; Pesarin & Salmaso, 2010). To produce an accurate approximate estimation of the permutation distribution, these tests are conducted using $B = 10,000$ permutations (Marozzi, 2004). Depending on the result of a Levene's test (Levene, 1961) (used to assess the homogeneity between the group variances) the Monte Carlo permutation tests are performed based on one of the following two statistics (under the null hypothesis):

$$T_0^* = \frac{\overline{X}_1 - \overline{X}_2}{\sqrt{\frac{S_1^2}{n_1} + \frac{S_2^2}{n_2}}}, p_{Levene's\ test} < 0.05 \qquad T_0^* = \frac{\overline{X}_1 - \overline{X}_2}{\sqrt{S_p\left(\frac{1}{n_{HC}} + \frac{1}{n_{SZ}}\right)}}, otherwise \qquad (6)$$

where $\overline{X}_1$ and $\overline{X}_2$ are the random sample means, S_1 and S_2 are the random sample standard deviations and n_1 and n_2 are the sample sizes for the groups 1 and 2, respectively. The pooled random standard deviation, S_p, is given by $S_p = \left((n_1 - 1)S_1^2 + (n_2 - 1)S_2^2\right)/(n_1 + n_2 - 2)$. Under the null

hypothesis, the statistic from Eq. (6) used to perform the statistical test is subsequently used to obtain the value of the statistic under each of the B permutations of the sample data.

The standard deviation of the difference of group means is estimated using 500 bootstrap samples within each permutation sample. This is performed so that the estimation of this quantity is conducted independently of the calculated means difference.

To complement the statistical hypothesis tests and understand the magnitude of the detected intergroup differences independently of the sample size, the effect size is estimated using Hedge's g statistic (Hedges, 1981). The use of this measure is based on its appropriateness to measure the effect size for the difference between means and to account for the size of the sample from each group.

4.7. Correction for multiple comparisons

We first investigate the fractional occupancy and dwell time of PL states across the range of clustering solutions to understand whether the occurrence and/or lifetime of states depends upon the condition. To achieve this, for a given partition model with K clusters, we perform K hypothesis tests following the procedure described in Section 2.9. Regarding the hypothesis tests, we consider three distinct significance thresholds: (1) the usual 5% significance level, $\alpha_1 = 0.05$; (2) a Bonferroni corrected significance threshold of $\alpha_2 = 0.05/K$ and (3) a conservative significance threshold of $\alpha_3 = 0.05/\sum_{K=2}^{20} K$.

4.8. Coupling Modes in 3D volumes

To visualize the coupling modes in axial slices and render the modes in transparent brains, we take all the 3D fMRI brain volumes aligned in MNI space and resize them to a spatial resolution of $10mm^3$ cubic voxels using linear interpolation (this step is needed to reduce the number of brain voxels V to a size supported by the hardware for VxV matrix decompositions). We subsequently get the *timeseries* from the V=1718 voxels inside a template MNI brain mask and compute the Hilbert transform of each voxel *timeseries*. We then get the leading eigenvectors in voxel space at each time point, resulting in 180954 leading eigenvectors, each with size 1x1718.

We identify all the points assigned to a given cluster obtained previously with LEiDA, and average all the 1x1718 leading eigenvectors obtained for the same time points, obtaining in this way a representation of the centroids in voxel space. These centroids are then placed back in the $10mm^3$ brain mask volume and reshaped into $2mm^3$ cubic voxels using linear interpolation, resulting in a representation of each cluster centroid in a 91x109x91 volume.

Data Availability

All fMRI data used in this study is from Autism Brain Imaging Data Exchange (ABIDE) (Craddock et al., 2013) released under the Preprocessed Connectomes Project (PCP) and available at http://preprocessed-connectomes-project.org/abide/index.html.

Code Availability

Source Code for the replication of the analysis and figure generation are made available as Matlab scripts (https://github.com/PSYMARKER/leida-matlab). The LEiDA Toolbox is also available in Python (https://github.com/PSYMARKER/leida-python/tree/dev).

Acknowledgements

Data collection and sharing for this project was funded by the Autism Brain Imaging Data Exchange (ABIDE) initiative. ABIDE I represents the first ABIDE initiative, involving numerous international sites that shared previously collected resting-state functional magnetic resonance imaging (R-fMRI), anatomical, and phenotypic datasets with the broader scientific community. The ABIDE dataset is publicly shared through the COINS Data Exchange application, a web-based data-sharing environment where researchers can browse the extensive COINS database for data related to their research. Requests to share data can then be made to the data's owner. The Preprocessed Connectomes Project (PCP) has also released preprocessed neuroimaging data from ABIDE, making it accessible to researchers worldwide. The ABIDE initiative is a consortium of the International Neuroimaging Data-sharing Initiative (INDI), aiming to accelerate our understanding of the neural bases of autism by aggregating and openly sharing neuroimaging data collected from laboratories around the world.

JC is supported by La Caixa Foundation, Spain (LCF/BQ/PR22/11920014) and the Foundation for Science and Technology, Portugal (UIDB/50026/2020, UIDP/50026/2020).

Ethics declarations

Data Usage and Ethical Compliance

This study utilized publicly available neuroimaging data from the Autism Brain Imaging Data Exchange (ABIDE), which is hosted under the Preprocessed Connectomes Project (PCP). The data were collected and shared by the contributing institutions in compliance with their respective ethical guidelines and informed consent protocols, ensuring participants' privacy and confidentiality.

Conflict of Interest

The authors declare no conflicts of interest in relation to the current study.

References

Aggarwal, C. C., & Reddy, C. K. (2018). *Data Clustering: Algorithms and Applications*. CRC Press.

Alonso Martínez, S., Deco, G., Ter Horst, G. J., & Cabral, J. (2020). The Dynamics of Functional Brain Networks Associated With Depressive Symptoms in a Nonclinical Sample. *Frontiers in Neural Circuits*, *14*, 570583.

Amemiya, S., Takao, H., Hanaoka, S., & Abe, O. (2023). Resting-state networks representation of the global phenomena. *Frontiers in Neuroscience*, *17*, 1220848.

Biswal, B. B., Mennes, M., Zuo, X.-N., Gohel, S., Kelly, C., Smith, S. M., Beckmann, C. F., Adelstein, J. S., Buckner, R. L., Colcombe, S., Dogonowski, A.-M., Ernst, M., Fair, D., Hampson, M., Hoptman, M. J., Hyde, J. S., Kiviniemi, V. J., Kötter, R., Li, S.-J., … Milham, M. P. (2010). Toward discovery science of human brain function. *Proceedings of the National Academy of Sciences of the United States of America*, *107*(10), 4734–4739.

Cabral, J., Fernandes, F. F., & Shemesh, N. (2023). Intrinsic macroscale oscillatory modes driving long range functional connectivity in female rat brains detected by ultrafast fMRI. *Nature Communications*, *14*(1), 375.

Cabral, J., Vidaurre, D., Marques, P., Magalhães, R., Silva Moreira, P., Miguel Soares, J., Deco, G., Sousa, N., & Kringelbach, M. L. (2017). Cognitive performance in healthy older adults relates to spontaneous switching between states of functional connectivity during rest. *Scientific Reports*, *7*(1), 5135.

Cahart, M.-S., Dell'Acqua, F., Giampietro, V., Cabral, J., Timmers, M., Streffer, J., Einstein, S., Zelaya, F., Williams, S. C. R., & O'Daly, O. (2022). Test-retest reliability of time-varying patterns of brain activity across single band and multiband resting-state functional magnetic resonance imaging in healthy older adults. *Frontiers in Human Neuroscience*, *16*, 980280.

Chen, J. E., Lewis, L. D., Chang, C., Tian, Q., Fultz, N. E., Ohringer, N. A., Rosen, B. R., & Polimeni, J. R. (2020). Resting-state "physiological networks." *NeuroImage*, *213*, 116707.

Craddock, C., Benhajali, Y., Chu, C., Chouinard, F., Evans, A., Jakab, A., Khundrakpam, B. S., Lewis, J. D., Li, Q., Milham, M., & Others. (2013). The neuro bureau preprocessing initiative: open sharing of preprocessed neuroimaging data and derivatives. *Frontiers in Neuroinformatics*, *7*(27), 5.

de Alteriis, G., Sherwood, O., Ciaramella, A., Leech, R., Cabral, J., Turkheimer, F. E., & Expert, P. (2024). DySCo: a general framework for dynamic Functional Connectivity. In *bioRxiv*.

https://doi.org/10.1101/2024.06.12.598743

Di Martino, A., Yan, C.-G., Li, Q., Denio, E., Castellanos, F. X., Alaerts, K., Anderson, J. S., Assaf, M., Bookheimer, S. Y., Dapretto, M., Deen, B., Delmonte, S., Dinstein, I., Ertl-Wagner, B., Fair, D. A., Gallagher, L., Kennedy, D. P., Keown, C. L., Keysers, C., … Milham, M. P. (2014). The autism brain imaging data exchange: towards a large-scale evaluation of the intrinsic brain architecture in autism. *Molecular Psychiatry*, *19*(6), 659–667.

Farinha, M., Amado, C., Morgado, P., & Cabral, J. (2022). Increased Excursions to Functional Networks in Schizophrenia in the Absence of Task. *Frontiers in Neuroscience*, *16*, 821179.

Fasano, M. C., Cabral, J., Stevner, A., Vuust, P., Cantou, P., Brattico, E., & Kringelbach, M. L. (2023). The early adolescent brain on music: Analysis of functional dynamics reveals engagement of orbitofrontal cortex reward system. *Human Brain Mapping*, *44*(2), 429–446.

Figueroa, C. A., Cabral, J., Mocking, R. J. T., Rapuano, K. M., van Hartevelt, T. J., Deco, G., Expert, P., Schene, A. H., Kringelbach, M. L., & Ruhé, H. G. (2019). Altered ability to access a clinically relevant control network in patients remitted from major depressive disorder. *Human Brain Mapping*, *40*(9), 2771–2786.

Fornito, A., Zalesky, A., & Breakspear, M. (2015). The connectomics of brain disorders. *Nature Reviews. Neuroscience*, *16*(3), 159–172.

Fox, M. D., & Raichle, M. E. (2007). Spontaneous fluctuations in brain activity observed with functional magnetic resonance imaging. *Nature Reviews. Neuroscience*, *8*(9), 700–711.

Friston, K. J., Williams, S., Howard, R., Frackowiak, R. S., & Turner, R. (1996). Movement-related effects in fMRI time-series. *Magnetic Resonance in Medicine*, *35*(3), 346–355.

Guthrie, W., Swineford, L. B., Nottke, C., & Wetherby, A. M. (2013). Early diagnosis of autism spectrum disorder: stability and change in clinical diagnosis and symptom presentation. *Journal of Child Psychology and Psychiatry, and Allied Disciplines*, *54*(5), 582–590.

Hancock, F., Rosas, F. E., McCutcheon, R. A., Cabral, J., Dipasquale, O., & Turkheimer, F. E. (2023). Metastability as a candidate neuromechanistic biomarker of schizophrenia pathology. *PloS One*, *18*(3), e0282707.

Hedges, L. V. (1981). Distribution theory for Glass's estimator of effect size and related estimators. *Journal of Educational Statistics*, *6*(2), 107–128.

Hodges, H., Fealko, C., & Soares, N. (2020). Autism spectrum disorder: definition, epidemiology, causes, and

clinical evaluation. *Translational Pediatrics*, *9*(Suppl 1), S55–S65.

Katsumi, Y., Zhang, J., Chen, D., Kamona, N., Bunce, J. G., Hutchinson, J. B., Yarossi, M., Tunik, E., Dickerson, B. C., Quigley, K. S., & Barrett, L. F. (2023). Correspondence of functional connectivity gradients across human isocortex, cerebellum, and hippocampus. *Communications Biology*, *6*(1), 401.

Knyazev, G. G., Savostyanov, A. N., Bocharov, A. V., Levin, E. A., & Rudych, P. D. (2020). Intrinsic Connectivity Networks in the Self- and Other-Referential Processing. *Frontiers in Human Neuroscience*, *14*, 579703.

Lee, T.-W. (1998). Independent Component Analysis. In *Independent Component Analysis* (pp. 27–66). Springer US.

Levene, H. (1961). *Robust tests for equality of variances*. 279–292.

Liu, X., Zhang, N., Chang, C., & Duyn, J. H. (2018). Co-activation patterns in resting-state fMRI signals. *NeuroImage*, *180*(Pt B), 485–494.

Li, W., Mai, X., & Liu, C. (2014). The default mode network and social understanding of others: what do brain connectivity studies tell us. *Frontiers in Human Neuroscience*, *8*, 74.

Lord, L.-D., Expert, P., Atasoy, S., Roseman, L., Rapuano, K., Lambiotte, R., Nutt, D. J., Deco, G., Carhart-Harris, R. L., Kringelbach, M. L., & Cabral, J. (2019). Dynamical exploration of the repertoire of brain networks at rest is modulated by psilocybin. *NeuroImage*, *199*, 127–142.

Marozzi, M. (2004). Some remarks about the number of permutations one should consider to perform a permutation test. *Statistica*, *64*(1), 193–201.

Newman, M. E. J. (2006). Finding community structure in networks using the eigenvectors of matrices. *Physical Review. E, Statistical, Nonlinear, and Soft Matter Physics*, *74*(3 Pt 2), 036104.

Oberman, L. M., & Kaufmann, W. E. (2020). Autism Spectrum Disorder Versus Autism Spectrum Disorders: Terminology, Concepts, and Clinical Practice. *Frontiers in Psychiatry*, *11*, 484.

Olsen, A. S., Lykkebo-Valløe, A., Ozenne, B., Madsen, M. K., Stenbæk, D. S., Armand, S., Mørup, M., Ganz, M., Knudsen, G. M., & Fisher, P. M. (2022). Psilocybin modulation of time-varying functional connectivity is associated with plasma psilocin and subjective effects. *NeuroImage*, *264*, 119716.

Pesarin, F., & Salmaso, L. (2010). *Permutation Tests for Complex Data: Theory, Applications and Software*. John Wiley & Sons.

Ronde, M., van der Zee, E. A., & Kas, M. J. H. (2024). Default mode network dynamics: An integrated

neurocircuitry perspective on social dysfunction in human brain disorders. *Neuroscience and Biobehavioral Reviews*, *164*(105839), 105839.

Sporns, O. (2018). Graph theory methods: applications in brain networks. *Dialogues in Clinical Neuroscience*, *20*(2), 111–121.

Stark, E. A., Cabral, J., Riem, M. M. E., Van IJzendoorn, M. H., Stein, A., & Kringelbach, M. L. (2020). The Power of Smiling: The Adult Brain Networks Underlying Learned Infant Emotionality. *Cerebral Cortex (New York, N.Y. : 1991)*, *30*(4), 2019–2029.

The Default Mode Network in Autism. (2017). *Biological Psychiatry: Cognitive Neuroscience and Neuroimaging*, *2*(6), 476–486.

Vidaurre, D., Abeysuriya, R., Becker, R., Quinn, A. J., Alfaro-Almagro, F., Smith, S. M., & Woolrich, M. W. (2018). Discovering dynamic brain networks from big data in rest and task. *NeuroImage*, *180*(Pt B), 646–656.

Vohryzek, J., Deco, G., Cessac, B., Kringelbach, M. L., & Cabral, J. (2020). Ghost Attractors in Spontaneous Brain Activity: Recurrent Excursions Into Functionally-Relevant BOLD Phase-Locking States. *Frontiers in Systems Neuroscience*, *14*, 20.

Washington, S. D., Gordon, E. M., Brar, J., Warburton, S., Sawyer, A. T., Wolfe, A., Mease-Ference, E. R., Girton, L., Hailu, A., Mbwana, J., Gaillard, W. D., Kalbfleisch, M. L., & VanMeter, J. W. (2014). Dysmaturation of the default mode network in autism: Dysmaturation of Default Network in Autism. *Human Brain Mapping*, *35*(4), 1284–1296.

Xie, H., Zheng, C. Y., Handwerker, D. A., Bandettini, P. A., Calhoun, V. D., Mitra, S., & Gonzalez-Castillo, J. (2019). Efficacy of different dynamic functional connectivity methods to capture cognitively relevant information. *NeuroImage*, *188*, 502–514.

Yeo, B. T. T., Krienen, F. M., Sepulcre, J., Sabuncu, M. R., Lashkari, D., Hollinshead, M., Roffman, J. L., Smoller, J. W., Zöllei, L., Polimeni, J. R., Fischl, B., Liu, H., & Buckner, R. L. (2011). The organization of the human cerebral cortex estimated by intrinsic functional connectivity. *Journal of Neurophysiology*, *106*(3), 1125–1165.